ARL-TR-10002 ● Oct 2024

A Computational Study on the Effect of Initial Powder Packing Configuration on Final Sintered Part Microstructures

by Brennan Watkins, Efrain Hernandez-Rivera, and Matthew Guziewski

NOTICES

Disclaimers

The findings in this report are not to be construed as an official Department of the Army position unless so designated by other authorized documents.

Citation of manufacturer's or trade names does not constitute an official endorsement or approval of the use thereof.

Destroy this report when it is no longer needed. Do not return it to the originator.

ARL-TR-10002 ● OCT 2024

A Computational Study on the Effect of Initial Powder Packing Configuration on Final Sintered Part Microstructures

Brennan Watkins
Colorado State University

Efrain Hernandez-Rivera and Matthew Guziewski
DEVCOM Army Research Laboratory

REPORT DOCUMENTATION PAGE

1. REPORT DATE	2. REPORT TYPE	3. DATES COVERED	
		START DATE	END DATE
October 2024	Technical Report	June 2023	August 2023

4. TITLE AND SUBTITLE
A Computational Study on the Effect of Initial Powder Packing Configuration on Final Sintered Part Microstructures

5a. CONTRACT NUMBER	5b. GRANT NUMBER	5c. PROGRAM ELEMENT NUMBER
5d. PROJECT NUMBER AH80	**5e. TASK NUMBER**	**5f. WORK UNIT NUMBER**

6. AUTHOR(S)
Brennan Watkins, Efrain Hernandez-Rivera, and Matthew Guziewski

7. PERFORMING ORGANIZATION NAME(S) AND ADDRESS(ES)	8. PERFORMING ORGANIZATION REPORT NUMBER
DEVCOM Army Research Laboratory ATTN: FCDD-RLA-MB Aberdeen Proving Ground, MD 21005-5066	ARL-TR-10002

9. SPONSORING/MONITORING AGENCY NAME(S) AND ADDRESS(ES)	10. SPONSOR/MONITOR'S ACRONYM(S)	11. SPONSOR/MONITOR'S REPORT NUMBER(S)

12. DISTRIBUTION/AVAILABILITY STATEMENT
DISTRIBUTION STATEMENT A. Approved for public release: distribution unlimited.

13. SUPPLEMENTARY NOTES
ORCIDs: Brennan Watkins, 0009-0005-1251-0694; Efrain Hernandez-Rivera, 0000-0002-7855-1027; Matthew Guziewski, 0000-0002-5761-720X

14. ABSTRACT
Sintering processes are widely used for manufacturing parts from powders of different material classes (e.g., ceramics). Many component properties critical to performance (e.g., porosity) depend on the initial powder packing configuration, sintering time, temperature, and pressure. The relationship between the initial powder packing configuration and the final part microstructure are poorly understood, leaving much to be gained from a comprehensive computational investigation of the topic. Furthermore, a large-scale experimental study of the packing-microstructure relationship would be prohibitively costly and time-consuming to conduct, whereas detailed simulation of a wide array of packing situations and sintering conditions can be easily carried out. Initial powder packing configurations were created using discrete element modeling via the LAMMPS package, and a Monte Carlo-based sintering model was subsequently used to simulate the densification of the part. However, the accuracy and speed of these methods depend on parameters such as domain size, time step size, and discretization mesh density; accordingly, convergence tests are performed on both the powder packing model and the sintering model to determine optimal simulation parameters. These developments permit expedient and accurate simulation of both powder packing and sintering processes, allowing for prediction of final part microstructures from initial powder packing configurations.

15. SUBJECT TERMS
sintering, packing, discrete element, Monte Carlo, microstructure, Sciences of Extreme Materials

16. SECURITY CLASSIFICATION OF:			17. LIMITATION OF ABSTRACT	18. NUMBER OF PAGES
a. REPORT	b. ABSTRACT	C. THIS PAGE		
UNCLASSIFIED	UNCLASSIFIED	UNCLASSIFIED	UU	33

19a. NAME OF RESPONSIBLE PERSON	19b. PHONE NUMBER *(Include area code)*
Efrain Hernandez-Rivera	410-306-4961

STANDARD FORM 298 (REV. 5/2020)
Prescribed by ANSI Std. Z39.18

Contents

List of Figures

Acknowledgments

This work was supported in part by high-performance computing (HPC) resources from the US Department of Defense (DOD) HPC Modernization Program, in collaboration with an appointment to the HPC Internship Program administered by the Oak Ridge Institute for Science and Education (ORISE) through an interagency agreement between the US Department of Energy (DOE) and the DOD. ORISE is managed by Oak Ridge Associated Universities (ORAU) under DOE contract number DE-SC0014664. All opinions expressed in this work are the authors' and do not necessarily reflect the policies and views of the DOD, DOE, or ORAU/ORISE.

1. Introduction

Sintering, a process used for creating solid components from powders, is widely used in manufacturing. Although sintering is used for metals, polymers, ceramics and composites, it is a preferred manufacturing technique for ceramic components due to their brittleness and high melting temperatures. Sintering is a solid-state process; that is, the powder particles are fused into a bulk material through the application of heat (and generally pressure), without melting. Furthermore, this process densifies the material, removing porosity as the particles fuse together. Thus, the final microstructure of the part is highly dependent on the sintering temperature, pressure, and duration as well as the initial packing configuration of the powder particles in the mold.

For ceramics, near-zero porosity is critical for the preservation of desirable mechanical properties: pores reduce the cross-sectional area of a part, increasing the stress concentration it experiences for a given loading state, resulting in nucleation sites for cracks. Refined grain microstructures are also generally desired for high strength, as prescribed by the Hall–Petch effect. Optimizing these properties can be difficult, because the long sintering times needed for full consolidation often produce large grains.[1]

Due to financial and time constraints associated with experimental work, it is desirable to design a high-throughput computational model for predicting part characteristics as a function of several input parameters (e.g., powder characteristics and sintering time). This method uses existing high-performance computing (HPC) resources to make connections between the initial powder characteristics and the final part microstructure. Accordingly, it is necessary to accurately and efficiently model both the initial packing of the powder in the mold—to form the green body compact—and the subsequent sintering of the green part into a densified component.

Generating synthetic green body compacts remains a computational challenge, especially for non-monomodal particle size distributions. As the size difference between the largest and smallest particles increases, the total number of particles rises sharply and dramatically increases the computational cost of simulating interparticle interactions, even when a simple contact model is used. A packing algorithm recently used by Srivastava et al.[2] yielded estimates for packing efficiency in bidisperse (two particle sizes present in the simulation) frictional arrangements of spheres. The maximum packing efficiency achieved in this work was reported to be approximately 0.87 for frictionless spheres with size dispersions up to 40:1, which occurred when the cumulative volume fraction (CVF) of small

particles in the mixture was approximately 0.26. Packing efficiencies for spheres with sliding friction ($\mu_s = 0.30$) were reduced slightly, showing a peak value of approximately 0.85. Subsequently, a frictionless model[3] was extended to power-law size distributions using an improved neighbor binning algorithm, managing to simulate powder packings with size dispersions up to 100:1.

Starting from the green body compact, the sintering process can be modeled using methods derived from Monte Carlo simulation.[4] These simulations have been parameterized to match experimental findings for copper powder sintering,[5] showing promise for direct application to higher temperature ceramic-sintering processes; furthermore, these Monte Carlo simulations have been used to predict the strain within sintered components that arise from vacancy annihilation.[6]

In this work, both a discrete-element powder packing model and a Monte Carlo-based sintering model were implemented. To generate accurate results without unnecessary computational expense, convergence tests were conducted to determine the appropriate simulation cell size, time step size, and total number of time steps for the powder packing model. The discrete-element model was also used to investigate the effects of particle size ratio, CVF, and sliding friction coefficient on the packing efficiency in systems with bidisperse and tridisperse size distributions. For the sintering model, the number of time steps and the discretization mesh density were varied to establish a relationship between the two parameters.

2. Materials and Methods

In this section, we outline the method used to generate the synthetic green bodies, which are based on discrete element modeling. Two techniques are explored: granular pouring and confinement packing. The former more readily follows physics-defined interactions, whereas the latter is more efficient. Furthermore, a brief description of the sintering model is presented.

2.1 Discrete Element Modeling

To understand the impact of powder characteristics (i.e., particle size distribution) on the initial particle packing configuration within a mold, a granular material simulation was constructed using the Large-scale Atomic/Molecular Massively Parallel Simulator (LAMMPS)[7] developed by Sandia National Laboratories. The simulation used in this work—a frictional sphere packing model—idealizes all powder particles as elastic spheres, which experience friction against the other particles and the walls of the container (wherever nonperiodic boundaries exist).

Elastic interactions between particles were simulated according to a Hertz–Mindlin contact model[8,9] via the LAMMPS hertz/material command. This model computes the force between particles i and j as

$$\vec{F}_{ij} = k_n \sqrt{R_{\text{eff}} \delta_{ij}^3} \hat{n} \,,$$

where k_n is the elastic stiffness of the material, $R_{\text{eff}} = R_i R_j / (R_i + R_j)$ is the effective interaction radius, and $\delta_{ij} = R_i + R_j - \left\| \vec{r}_{ij} \right\|$ is the particle overlap. Here, R_i and R_j are the radii of particles i and j, and $\vec{r}_{ij} = \vec{r}_i - \vec{r}_j$ is the separation between the particle centers. The direction vector for the interparticle force is $\hat{n} = \vec{r}_{ij} / \left\| \vec{r}_{ij} \right\|$.

In addition to elastic interactions, the Hertz–Mindlin contact model includes particle–particle and particle–container frictional interactions. For this work, only a nonzero tangential sliding friction was simulated, with a friction coefficient μ_s. Only nonperiodic simulation cell boundaries were modeled with frictional interactions; for periodic boundaries, no particle–container interaction was present.

The powder packing configurations were initially determined via a granular pouring model. This approach initiates particles at the top of a vertically elongated simulation cell and allows them to fall to the bottom due to gravity, as shown in Fig. 1. As more particles fall, they pile up at the bottom of the cell and eventually settle into a stable configuration. Once sufficient particles have been introduced, the simulation volume is truncated and a small number of additional time steps is allowed to elapse. Then, the lower 75% of the simulation volume is retained to isolate the most densely packed portion of the overall configuration, and this reduced volume is taken as the final powder packing configuration.

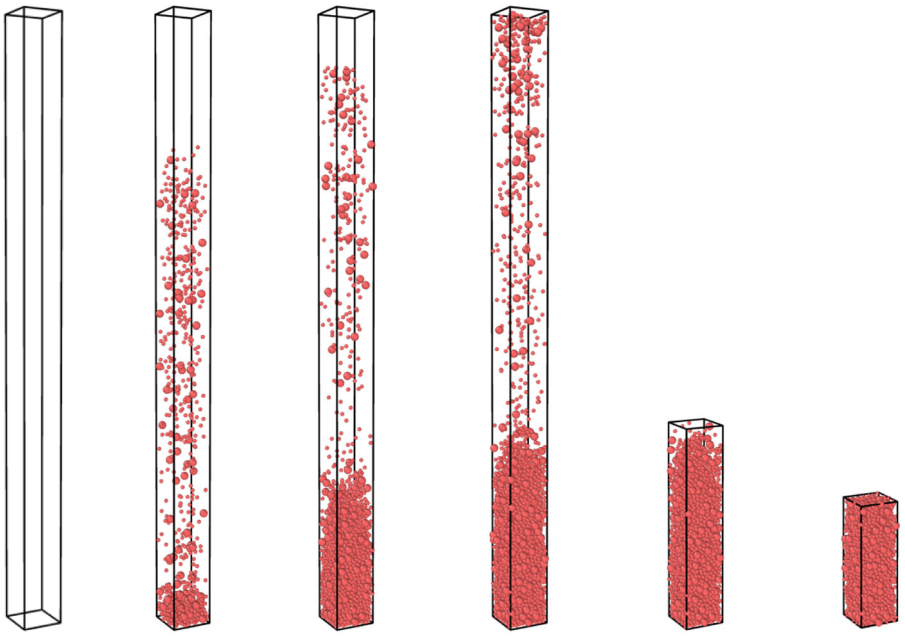

Fig. 1 Visualization of the granular pouring model

Following the work of Srivastava et al.[2] and Santos et al.,[10] a confinement-packing model was also implemented. This approach uses a very large initial simulation volume, populated randomly with particles, wherein overlapping particles are deleted and a small confinement pressure is applied to jam the particles together.

Figure 2 shows a $30 \times 30 \times 30R$ initial simulation volume that was selected to produce an approximately $10 \times 10 \times 10R$ final volume, where R is the radius of the largest powder particle in the mixture. The applied confinement pressure was chosen to be

$$P_{\mathrm{a}} = \frac{k_n \cdot 10^{-6}}{2R_{\mathrm{min}}},$$

where R_{min} is the radius of the smallest particle in the simulation. For a mono-sized set of particles, $R_{\mathrm{min}} = R$. The state of applied stress is purely hydrostatic; that is, $P_{\mathrm{a},xx} = P_{\mathrm{a},yy} = P_{\mathrm{a},zz} = P_{\mathrm{a}}$ and $P_{\mathrm{a},xy} = P_{\mathrm{a},yx} = P_{\mathrm{a},yz} = P_{\mathrm{a},zy} = P_{\mathrm{a},zx} = P_{\mathrm{a},xz} = 0$.

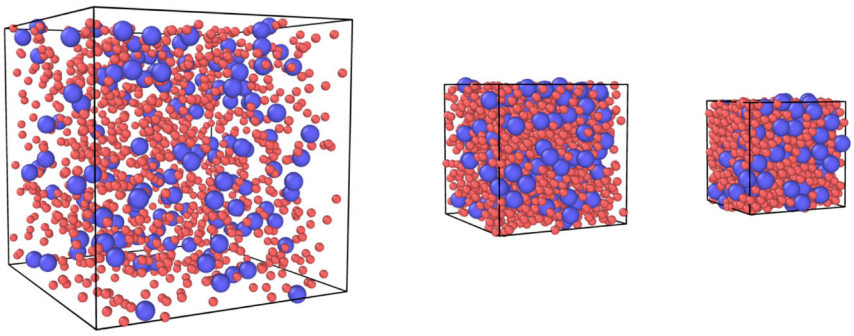

Fig. 2 Visualization of the confinement-packing model

2.1.1 Determination of Appropriate Simulation Cell Size

Due to the use of periodic boundary conditions in the LAMMPS simulation, an insufficiently large simulation volume can produce direct or indirect particle self-interaction, rendering the simulation unstable. To mitigate this effect, a convergence study was performed to determine the appropriate simulation cell size. This study entailed simulations of the same powder pouring process but with successively larger simulation cells in the x- and y-dimensions. The end-of-run packing efficiency, ϕ, was computed as an average of 10 simulations for each cell size; the mean final packing efficiency, μ_ϕ, and standard deviation in the final packing efficiency, σ_ϕ, were used to determine convergence. This process was subsequently repeated for the confinement-packing model.

2.1.2 Determination of Appropriate Time Step Size

Following the work of Monti et al.,[3] the appropriate time step size was assumed to depend on the smallest particle present in the mixture. If time steps are too large, excessively large particle displacements will be observed, which generate unrealistically high interparticle forces (i.e., very high particle velocities). This can prevent the simulation from ever converging to a stable packing arrangement, resulting in anomalously low packing efficiencies. Accordingly, the time step chosen was $\Delta t = \alpha\tau$, where α is a scaling coefficient (to be determined experimentally) and τ is defined as

$$\tau = \sqrt{\frac{M_{\min}}{k_n}},$$

where $M_{\min} = 4\pi\rho R_{\min}^3/3$ is the effective mass of the smallest particle present in the system, with ρ being the mass density of the particles. To estimate an appropriate α value for this work, several simulations with different α values were performed; the average and standard deviation of the packing efficiency were examined at each α value to determine adequate convergence. These simulations

were performed using the confinement-packing model, for both a mono-size distribution of particles and a bidisperse distribution with a 10:1 size ratio.

2.1.3 Determination of Appropriate Number of Time Steps

The acceptable number of time steps, $N_{\max}$, was determined using the same approach. Several otherwise-identical simulations with different $N_{\max}$ values were carried out, and convergence was gauged using μ_ϕ and σ_ϕ for 10 simulations at each $N_{\max}$ value.

2.2 Characterization of Powder Packing Configurations

Final powder packing configurations were characterized according to three separate metrics: packing efficiency, lacunarity, and Voronoi entropy. The packing efficiency was straightforwardly taken to be the cumulative volume of all particles present at the end of the simulation, normalized by the final volume of the simulation cell:

$$\phi = \frac{\sum V_i}{V_{\text{cell}}} = \frac{4}{3}\frac{\sum R_i^3}{V_{\text{cell}}}.$$

Here, V_i and R_i are the volume and radius of the i^{th} particle. Lacunarity, which can be thought of as a measure of inhomogeneity or texture, can be quantified by partitioning the simulation cell into subvolumes and counting the number of particle centers present within each subvolume. Using the work of Chekuryaev et al.[11] as a guide, the lacunarity parameter Λ was computed according to

$$\Lambda = \left(\frac{\sigma}{\mu}\right)^2,$$

where σ is the standard deviation in the number of particle centers found in each subvolume, and μ is the mean number of particle centers per subvolume. The Voronoi entropy was also computed for final powder packing configurations, via the following equation:

$$S = \sum_i P_i \ln P_i,$$

where P_i is the probability of a given Voronoi polyhedron having i faces. Generation of Voronoi polyhedra[12] was performed automatically in LAMMPS, which is shown in Fig. 3.

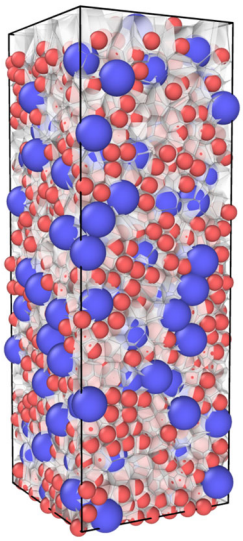

Fig. 3 Visualization of Voronoi polyhedra within a random sphere-packing arrangement

2.3 Monte Carlo Sintering Model

The sintering process was modeled using a Monte Carlo-based approach via the Stochastic Parallel PARticle Kinetic Simulator (SPPARKS) simulation package. The model developed for this work uses a rejection kinetic Monte Carlo algorithm to model three types of events—grain growth, pore migration, and pore annihilation—as the initial "green compact" is sintered into a bulk material.

The green compact modeled at the start of the SPPARKS sintering process is derived from the final powder packing configuration of a LAMMPS simulation. Each spherical particle is assumed to be a single crystal and is accordingly assigned a random "spin" to represent its crystallographic orientation. The SPPARKS sintering application discretizes the LAMMPS output configuration into a voxelized domain, where voxels are either filled (order parameter larger than 0) or unfilled (0) with material. The density of the discretized domain (or, alternatively, the number of voxels in the simulation cell) therefore has a pronounced effect on the behavior of the model. To characterize this effect, a series of SPPARKS simulations were performed with the spacing between mesh points, Δx, being varied. Each datum shown for these convergence tests is averaged over five SPPARKS runs with identical inputs. Figure 4 shows a representative sintering simulation, starting as perfect spheres and ending as a consolidated microstructural component. Note the initial increase in exterior roughness due to pore annihilation. Once the porosity has sufficiently decreased, grain growth becomes the dominant process.

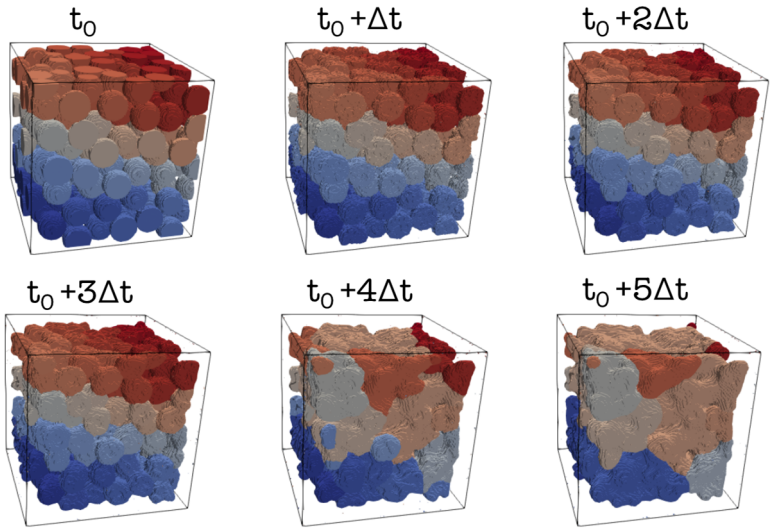

Fig. 4 Evolution of part microstructure within SPPARKS sintering simulation

In the sintering model, the total system energy is computed according to the work by Tikare et al.[5]:

$$E = \frac{1}{2}\sum_{i=1}^{N}\sum_{j=1}^{n} J_{ij}\left(1 - \delta(q_i, q_j)\right),$$

where N is the total number of sites (or voxels) in the simulation, n is the number of neighbors for each site, and $\delta(q_i, q_j)$ is the Kronecker delta applied to the state q_i of each site i and the states q_j of each of its neighbor sites j.

The frequency at which some event i is attempted is given by

$$\omega_i = \omega_{0,i} \exp\left(-\frac{E_i}{k_B T}\right),$$

where E_i is the activation energy for the event, $\omega_{0,i}$ is a constant prefactor, T is the temperature, and k_B is Boltzmann's constant. Each attempted process is then either accepted or rejected according to an acceptance probability given by

$$P_i^{\text{accept}} = \exp\left(-\frac{\alpha \Delta E}{k_B T}\right),$$

where ΔE is the global energy change resulting from the proposed event. The probability of event i occurring, then, is given by

$$P_i = \omega_i P_i^{\text{accept}} = \omega_{0,i} \exp\left(-\frac{E_i}{k_B T}\right) \exp\left(\frac{\alpha \Delta E}{k_B T}\right) = \omega_{0,i} \exp\left(-\frac{E_i + \alpha \Delta E}{k_B T}\right).$$

Accordingly, the SPPARKS sintering model takes as inputs the attempt rate prefactors for grain growth, pore migration, and pore annihilation ($\omega_{0,\mathrm{gg}}$, $\omega_{0,\mathrm{pm}}$, and $\omega_{0,\mathrm{pa}}$, respectively) and the event temperatures (β^1_{gg}, β^1_{pm}, and β^1_{pa}, where $\beta^1_i = \alpha_i\beta_i = \alpha_i/k_{\mathrm{B}}T$). For the purposes of the tests performed in this work, the E_i were set to zero, meaning that $\omega_i = \omega_{0,i}$; in the future, these values can be replaced with estimates for a particular material to give reasonable variation in event attempt rates with temperature.

In the sintering model, grain growth is proposed as a random alteration of the spin of a given filled site to that of one of the neighboring filled sites; the probability of acceptance of a grain growth event is computed as described above. Thus, over several time steps, the system will evolve to favor certain grains over others, allowing them to grow at the expense of their neighbors. Pore migration in the sintering model is also straightforward: an unfilled site is selected, and if it has a filled neighboring site, then the two sites may be exchanged. The newly filled site has its spin set to the most energetically favored grain orientation. Through this process, unfilled sites are allowed to break off from pores (agglomerations of unfilled sites) to form vacancies. The third process that was modeled is vacancy annihilation, which deals specifically with these isolated unfilled sites. To annihilate a vacancy, a path is defined from the vacancy to the outside surface of the part, passing through the center of mass of the nearest grain. All sites along the path, filled or unfilled, are then moved one position toward the vacancy, annihilating it and creating a vacant site at the surface of the part.

3. Results

Time and spatial domain tuning studies were performed to determine the ideal parameter settings for optimizing packing efficiency. Optimal conditions for mono-sized and bidisperse packing configurations were determined, which were used to generate idealized powder green bodies. A sample green body was then used to perform a mesh dependence study for the sintering simulations.

3.1 LAMMPS Sphere Packing Model Results

Close packing of mono-sized spheres produces a theoretical packing efficiency of approximately 0.74; however, random (frictionless) packing produces a packing efficiency of only approximately 0.64.[13–15] For the granular pouring model, the converged value is approximately 0.624, as shown in Fig. 5, which is lower than the theoretical maximum packing efficiency due to the inclusion of frictional interactions between particles. The end-of-run packing efficiency deviated wildly from this anticipated value when the minimum simulation cell dimension was

below about $6R$; beyond $10R$, the results were sufficiently converged, because the standard deviation in packing efficiency between runs dropped to below 1%. In addition, the variation between runs—arising from the random nature of the simulation—accounted for more variability than did the cell size, if the simulation cell was no smaller than approximately $10R$ in any dimension.

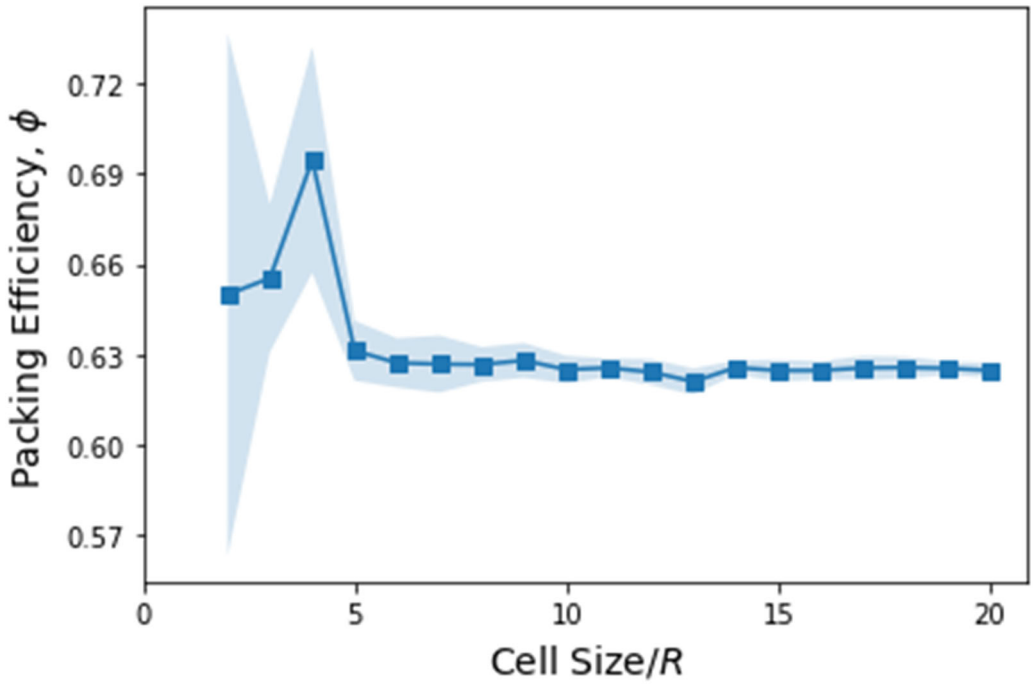

Fig. 5 Convergence of mono-sized sphere packing efficiency with respect to simulation cell size in the granular pouring. Bands show the standard deviation.

For the time step convergence, the acceptable time step multiplier value was approximately $\alpha = 0.10$; beyond this value, the mean packing efficiency settles to a value between 0.6291 and 0.6302, with the standard deviation in final packing efficiency between identical runs falling to approximately 0.002. This time step multiplier was sufficiently refined for both packing methods. Similarly, a cell size convergence study was performed for bidisperse particle sizes with the confinement packing model (Fig. 6). Again, good convergence is observed for a cell size of $6R$, with an average packing efficiency of 0.69.

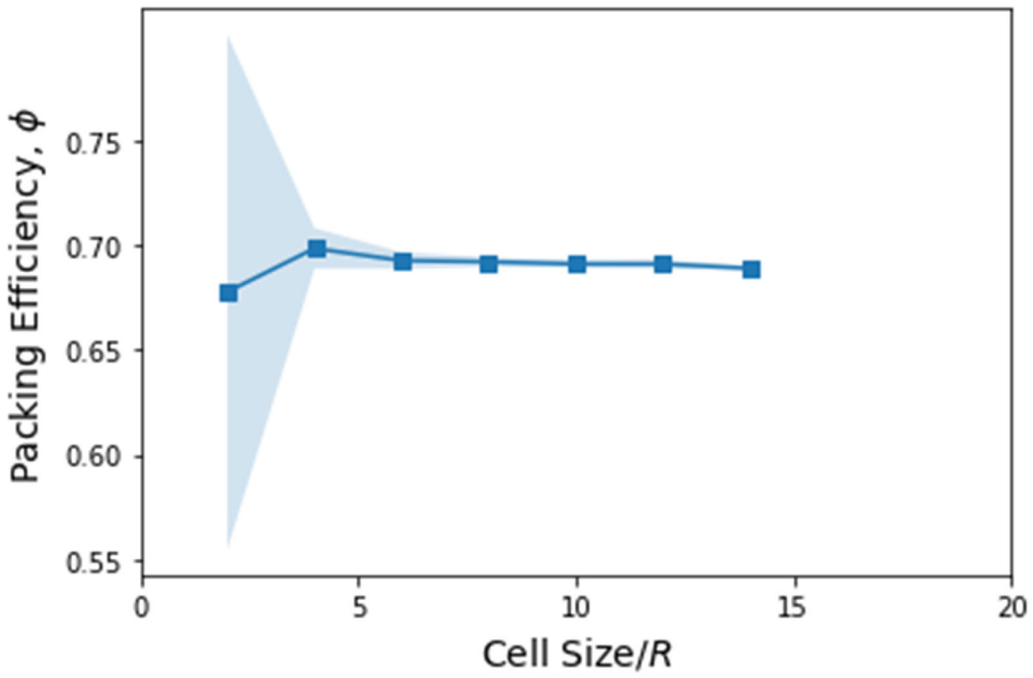

Fig. 6 Convergence of bidisperse spheres (5:1 size ratio) packing efficiency with respect to simulation cell size in the confinement packing models. Bands show the standard deviation.

For comparison, both the pouring model and the confinement-packing model were examined for convergence over a wide range of N_{max} values (Fig. 7). Using a very conservative time step ($\Delta t = 0.01\tau$), it is evident that the confinement-packing model converges very quickly to a stable packing efficiency: after approximately 1 million time steps, or $1 \times 10^4\tau$, ϕ has converged to approximately 0.624 (Fig. 7). By contrast, the pouring model fails to converge after 10^8 time steps, or $1 \times 10^6\tau$. Accordingly, the confinement-packing model was deemed superior to the pouring model, and the remainder of the LAMMPS simulation work was performed using the more efficient methodology.

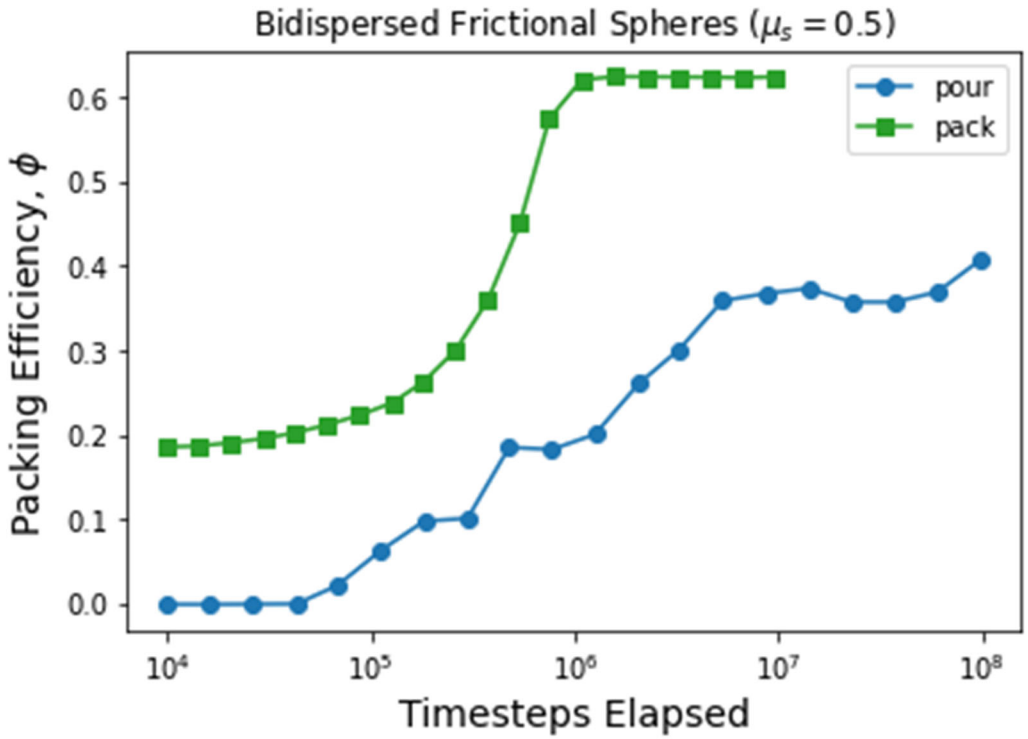

Fig. 7 Evolution of final packing efficiency with respect to total runtime of the granular pouring model (blue circles) and the confinement-packing model (green square). The confinement-packing model exhibits much faster convergence, even with a very conservative time step size ($\Delta t = 0.01\tau$). Both tests are for bidisperse frictional packings with a 2:1 particle size ratio.

As indicated by prior work on bidisperse packing of spheres,[2] the packing efficiency increases substantially as the size dispersion increases. Furthermore, an increase in the friction coefficient naturally reduces packing efficiencies. A corresponding reduction in the magnitude of the Voronoi entropy is seen as the simulations converge.

Even with the time step scaled according to the effective mass of the smallest particle in the system (see the Materials and Methods Section for details), a larger size dispersion contributes significantly to the computational cost of the simulation. The packing efficiency data in Fig. 8 show the 5:1 size ratio taking approximately tenfold more time steps than the 2:1 size ratio to converge, representing an enormous increase in resource consumption. Hence, the ability of the confinement-packing model to converge rapidly even with a conservative time step yields a significant advantage over the pouring model. Further results for various particle size dispersions, CVFs, and sliding friction coefficients are shown in the Appendix.

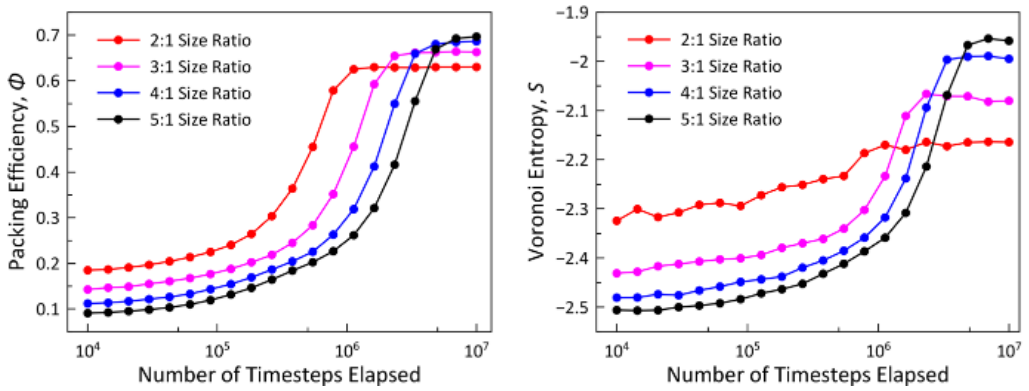

Fig. 8 Variation in packing efficiency and Voronoi entropy with respect to the number of allowed simulation time steps. Greater particle size dispersion contributes to both increased packing efficiency and lower (smaller magnitude) Voronoi entropy.

The lacunarity parameter was also computed for many of these packed configurations, showing the inhomogeneity of the particle mixture. As is evident from Fig. 9, the computed lacunarity is strongly dependent on the size of the subvolumes into which the sample is divided. When the subvolume is a very small portion of the simulation cell, the standard deviation in the number of particle centers per subvolume is large compared to the mean value, so the lacunarity parameter increases in magnitude rapidly. At the other extreme, if the simulation cell contains only one subvolume, then the lacunarity is zero. This size variation also means that there are variable measures of lacunarity that depend on which particles are included in the analysis. Figure 9 shows lacunarity values for the same structure—a 5:1 bidisperse arrangement of randomly packed spheres—computed with different subvolume sizes and counting choices. If only the large particles are counted, then the lacunarities are quite high, indicating a rough texture. However, if only the small particles are counted, far greater homogeneity is seen.

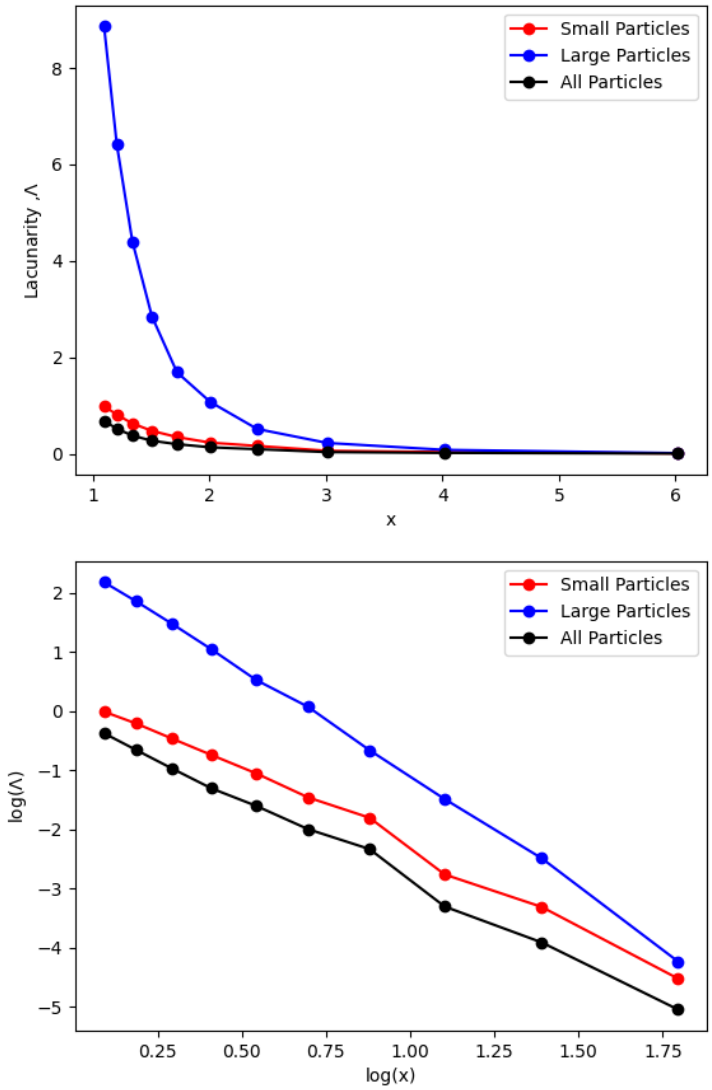

Fig. 9 Variation in lacunarity parameter *Λ* with subvolume edge length, x (as a multiple of the large particle radius *R*). The data is presented as a linear-linear plot (top) and as a log-log plot (bottom), showing the different values obtained from different particle center counting methods.

In addition to various bidisperse particle size distributions, a tridisperse size distribution with a 4:2:1 size ratio was modeled. As seen in Fig. 10, the sides of the ternary diagram are consistent with the bidisperse packing efficiency results. In the case of this size distribution, the maximum packing efficiency lies along the rightward side of the ternary (which represents an 8:1 bidisperse mixture). It is possible that, with greater size ratios, the optimal packing efficiency may shift away from the sides of the ternary; however, this was not pursued in the current work. These results broadly agree with experimental results of ternary mixtures of glass spheres,[16,17] which show that optimal packing is attained for bidispersed mixtures of large and small spheres (Fig. 10).

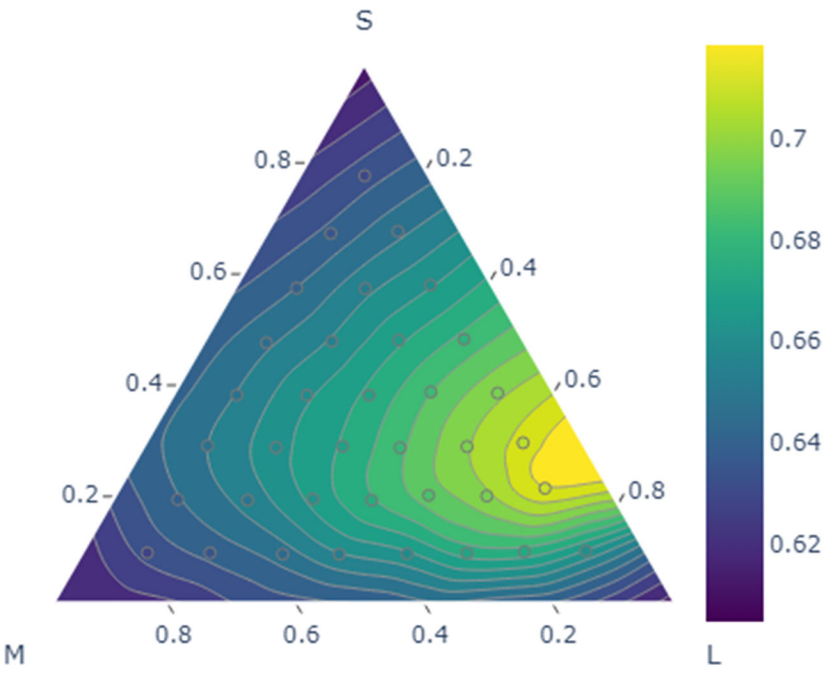

Fig. 10 Packing efficiency of powder with a tridisperse size distribution and a 4:2:1 size ratio. The terminal labels S, M, and L indicate the smallest, middle, and largest mono-size particle data, respectively.

3.2 SPPARKS Sintering Model Results

The convergence behavior of the SPPARKS model exhibited a strong dependence on the number of voxels in the simulation cell. Figure 11 shows the density of the part (relative to a bulk material) increasing over the course of the sintering simulations with different Δx values. It is evident from these results that an increase in the resolution of the discretization mesh dramatically increases the cost of the simulation. This is intuitive, because a halving of the mesh spacing results in an eightfold increase in the total number of mesh sites. If the mesh is too coarse (corresponding to a spacing of approximately $\Delta x \geq 0.25$), then significant variation appears between individual runs and the results become less stable.

The convergence speed with respect to the number of simulations time steps was initially assumed to trend roughly linearly with the total number of voxels, meaning that the mesh spacing Δx would have a cubic relationship with the required number of steps. To examine this possibility, the sintering curves were plotted against the number of time steps, N, scaled by the voxel volume, Δx^3. Figure 12 clearly shows that this relationship is not precisely linear, because the sintering curves do not appear to converge to a stable value as Δx is reduced. This implies that, although the number of required steps is somewhat volume-dependent, there are other dependencies that alter the overall behavior of the model. This is perhaps unsurprising, because processes such as grain growth will exhibit area dependence.

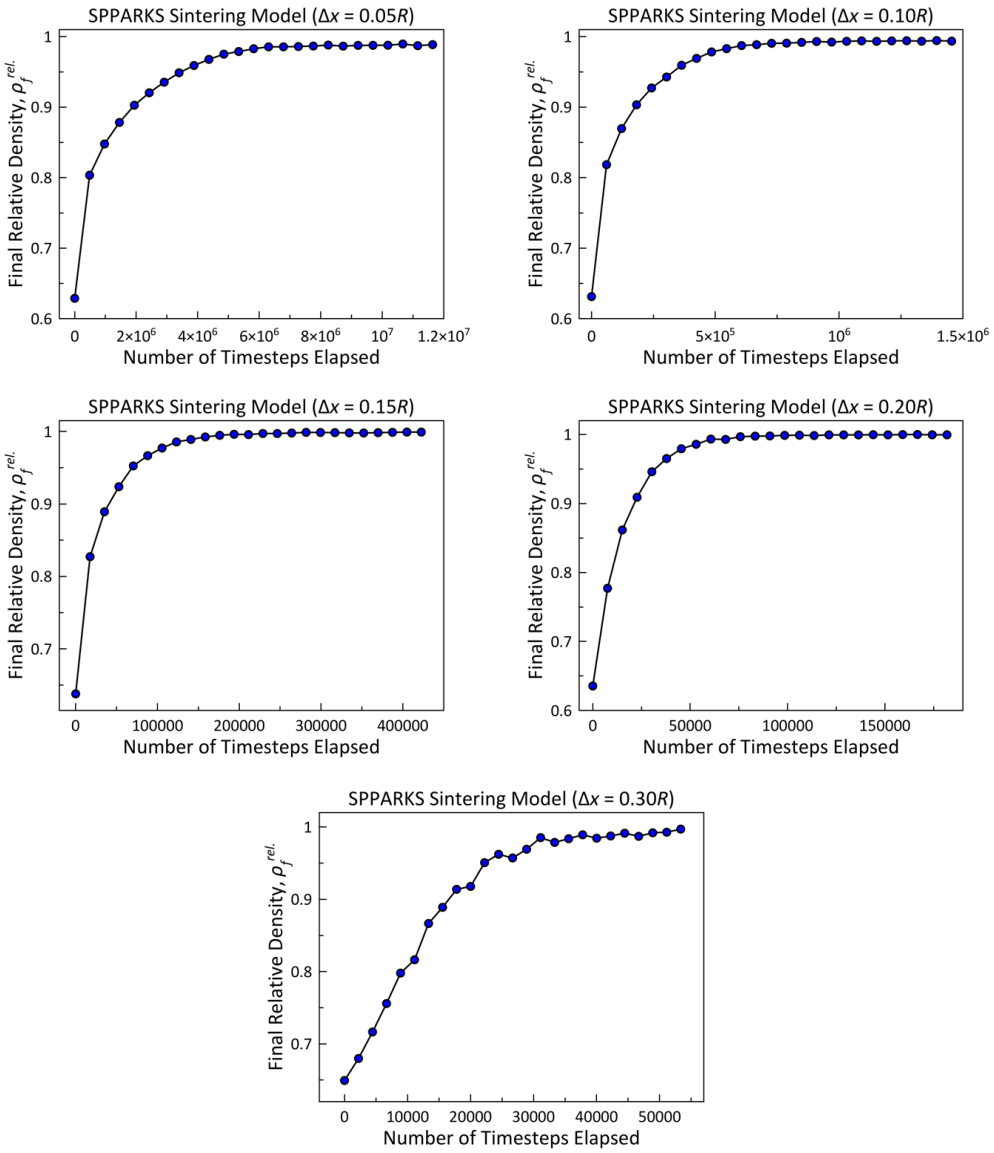

Fig. 11 SPPARKS sintering curves for different discretization mesh spacings, Δx. The denser meshes, having considerably more voxels, require a far larger number of time steps to converge. If the discretization is too coarse, the results become unstable.

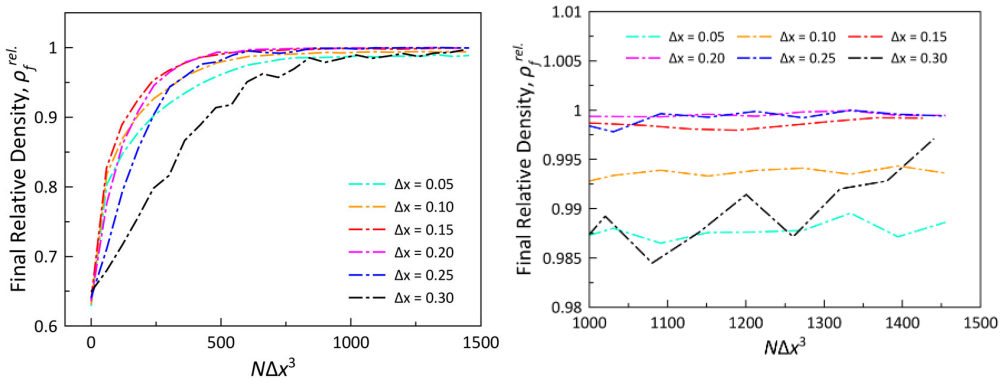

Fig. 12 Sintering curves scaled by voxel volume, showing similar behavior but convergence to slightly different final relative densities

4. Conclusions

Both of LAMMPS' powder packing models explored in this work (granular pouring and confinement-packing) produced realistic final packing configurations close to theoretical packing efficiencies for mono-sized sphere arrangements. However, the confinement-packing model was converged to reasonable estimates of packing efficiency in a smaller number of time steps than the granular pouring model, owing to the omission of the actual pouring and settling processes required for the latter model. Thus, the confinement-packing model can be used to generate reasonable estimates for packing efficiency, lacunarity, and Voronoi entropy without unnecessary resource use, allowing for far greater simulation throughput.

The confinement-packing model was used to generate estimates of powder packing efficiency over a range of friction coefficients, bidisperse particle size ratios, and CVFs, and it showed reasonably good agreement with prior work. Furthermore, the convergence tests demonstrated the necessity of allowing larger numbers of time steps in high-size-ratio simulations, accentuating the advantage of the confinement-packing model.

The discretization mesh density in SPPARKS had a dramatic influence on both the stability of the model's results and the required runtime for the simulation. The total number of mesh sites (or voxels) in the simulation space had a roughly linear effect on the required number of time steps, although other effects are present.

To fully implement the sintering model, it is necessary to fully characterize the model's dependence on the relative event probabilities by examining each type of event independently and in greater detail—the grain growth, pore migration, and vacancy annihilation processes have different responses to mesh refinement. Furthermore, available experimental data for common materials (e.g., alumina) should be used to give the event attempt rates reasonable temperature dependence;

ab initio or atomistic results may stand-in where experimental data are lacking. Completion of these additional tasks allows for rapid, reliable powder packing and sintering simulations, yielding a high-throughput computational asset for guiding future experiments.

5. References

1. Pan Y, Li H, Liu Y, Liu Y, Hu K, Wang N, Lu Z, Liang J, He S. Effect of holding time during sintering on microstructure and properties of 3D printed alumina ceramics. Front Mater. 2020;7:54. https://doi.org/10.3389/fmats.2020.00054

2. Srivastava I, Roberts SA, Clemmer JT, Silbert LE, Lechman JB, Grest GS. 2021. Jamming of bidisperse frictional spheres. Phys Rev Research. 2021;3(3):L032042. https://doi.org/10.1103/PhysRevResearch.3.L032042

3. Monti JM, Clemmer JT, Srivastava I, Silbert LE, Grest GS, Lechman JB. Large-scale frictionless jamming with power-law particle size distributions. Phys Rev E. 2022;106(3):034901. https://doi.org/10.1103/PhysRevE.106.034901

4. Tikare V, Braginsky M, Olevsky EA. Numerical simulation of solid-state sintering: I, sintering of three particles. JACerS. 2003;86(1):49–53. https://doi.org/10.1111/j.1151-2916.2003.tb03276.x

5. Tikare V, Braginsky M, Bouvard D, Vagnon A. 2010. Numerical simulation of microstructural evolution during sintering at the mesoscale in a 3D powder compact. Comput Mater Sci. 2010;48(2):317–325. https://doi.org/10.1016/j.commatsci.2010.01.013

6. Bjørk R, Frandsen HL, Tikare V, Olevsky E, Pryds N. 2014. Strain in the mesoscale kinetic Monte Carlo model for sintering. Comput Mater Sci. 2014;82:293–297. https://doi.org/10.1016/j.commatsci.2013.09.051

7. Plimpton S. 1995. Fast parallel algorithms for short-range molecular dynamics. J Comput Phys. 1994;117(1):1–19. https://doi.org/10.1006/jcph.1995.1039

8. Mindlin RD. Compliance of elastic bodies in contact. J Appl Mech. 1949;16(3):259–268. https://doi.org/10.1115/1.4009973

9. Mindlin RD, Deresiewicz H. Elastic spheres in contact under varying oblique forces. J Appl Mech. 1953;20(3):327–344. https://doi.org/10.1115/1.4010702

10. Santos AP, Bolintineanu DS, Grest GS, Lechman JB, Plimpton SJ, Srivastava I, Silbert LE. Granular packings with sliding, rolling, and twisting friction. Phys Rev E. 2020;102(3):032903. https://doi.org/10.1103/PhysRevE.102.032903

11. Chekuryaev AG, Sychov MM, Perevislov SN, Ulanov VN. Digital characteristics of microstructure of diamond—silicon carbide composites. Ceramics. 2023;6(2):1067–1077. https://doi.org/10.3390/ceramics6020063

12. Brostow W, Dussault J-P, Fox BL. Construction of Voronoi polyhedra. J Comput Phys. 1978;29(1):81–92. https://doi.org/10.1016/0021-9991(78)90110-9

13. Berryman JG. Random close packing of hard spheres and disks. Phys Rev A. 1983;1(27):1053. https://doi.org/10.1103/PhysRevA.27.1053

14. Torquato S, Truskett TM, Debenedetti PG. Is random close packing of spheres well defined? Phys Rev Lett. 2000;84(10):2064. https://doi.org/10.1103/PhysRevLett.84.2064

15. O'Hern CS, Silbert LE, Liu AJ, Nagel SR. Jamming at zero temperature and zero applied stress: the epitome of disorder. Phys Rev E. 2003;68(1):011306. https://doi.org/10.1103/PhysRevE.68.011306

16. Standish N, Collins DN. The permeability of ternary particulate mixtures for laminar flow. Powder Tech. 1983;36(1):55–60.

17. Leitzelement M, Lo CS, Dodds J. Porosity and permeability of ternary mixtures of particles. Powder Tech. 1985;41(2):159–164.

Appendix. Packing Efficiency Comparisons

Although particle size and volume fraction are the primary factors in determining packing efficiency, there are some kinetic effects that also play a role in determining the final configuration during these simulations. Chief among these is the coefficient of sliding friction, which controls how easily particles can move past each other. Figure A-1 shows the influence of this parameter on different particle size ratios, where variations of 3–4% in the packing efficiency can be observed. This provides another tool to help better align these simulation results with experimental packing of particles, with one such comparison shown in Figure A-2.

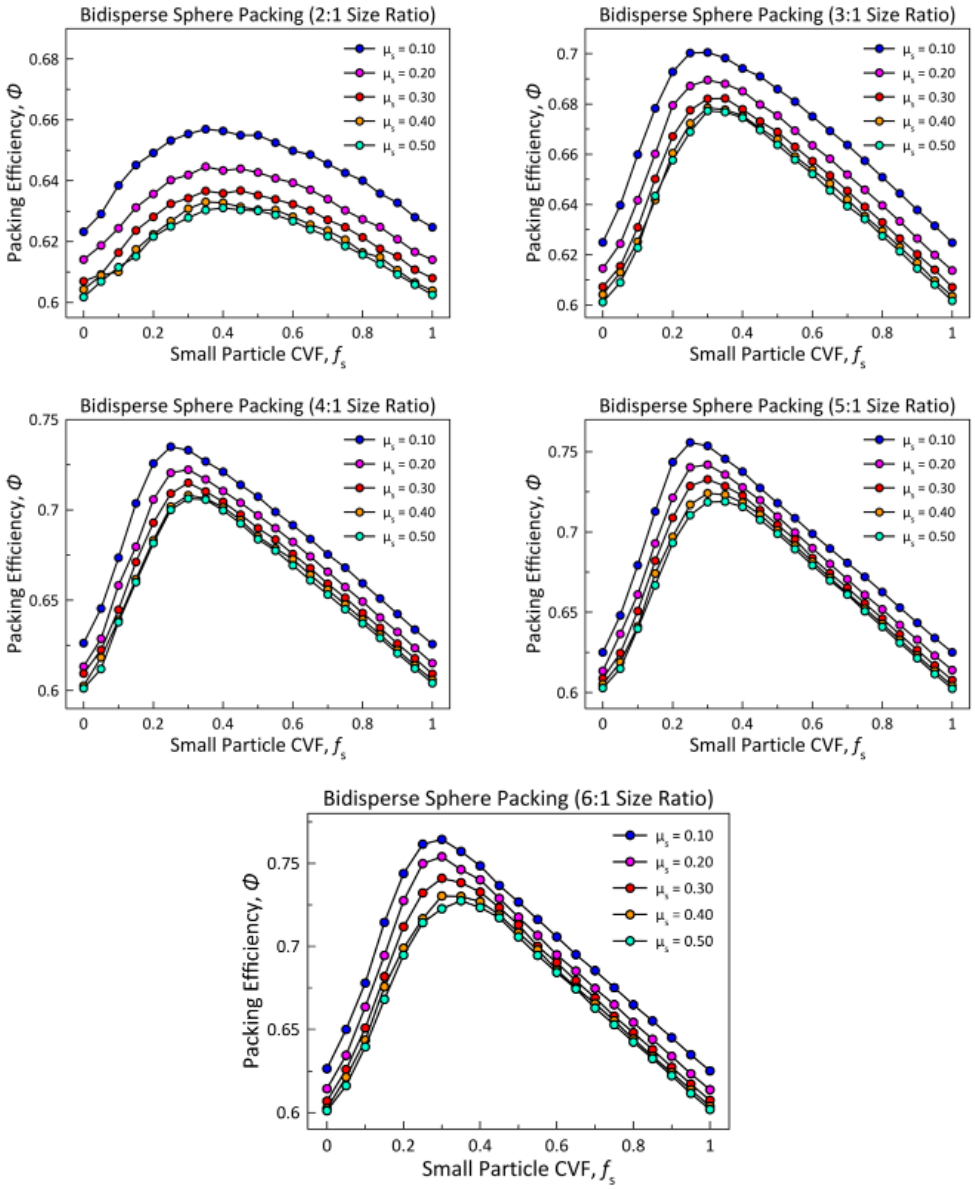

Fig. A-1 Comparison of packing efficiencies for various particle size dispersions, cumulative volume fractions, and sliding friction coefficients. Lower friction coefficients and higher size dispersions result in increased packing efficiency. The optimal cumulative volume fraction of small particles is always approximately 0.3, although it shows some variation.

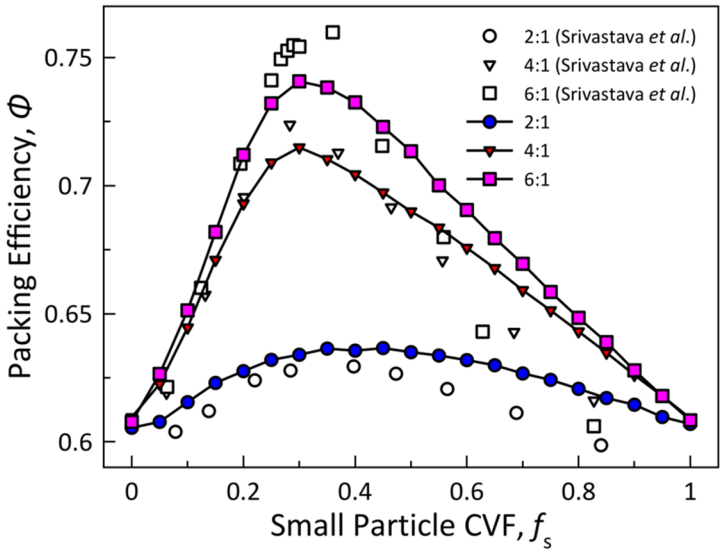

Fig. A-2 Comparison of packing efficiency results from Srivastava et al.[1] and the current work for bidisperse distributions of frictional elastic spheres with μ_s = 0.30

[1] Srivastava I, Roberts SA, Clemmer JT, Silbert LE, Lechman JB, Grest GS. 2021. Jamming of bidisperse frictional spheres. Phys Rev Research. 2021;3(3):L032042. doi:https://doi.org/10.1103/PhysRevResearch.3.L032042

List of Symbols, Abbreviations, and Acronyms

CVF	cumulative volume fraction
DOD	US Department of Defense
DOE	US Department of Energy
HPC	high-performance computing
LAMMPS	Large-scale Atomic/Molecular Massively Parallel Simulator
ORAU	Oak Ridge Associated Universities
ORISE	Oak Ridge Institute for Science and Education
SPPARKS	Stochastic Parallel PARticle Kinetic Simulator

1 (PDF)	DEFENSE TECHNICAL INFORMATION CTR DTIC OCA
1 (PDF)	DEVCOM ARL FCDD RLB CI TECH LIB